

Domain walls in single-chain magnetsVivien Pianet,^{1,2,3,4,*} Matias Urdampilleta,^{1,2} Thierry Colin,^{3,4,5} Rodolphe Clérac,^{1,2} and Claude Coulon^{1,2,†}¹*Univ. Bordeaux, CRPP, UPR 8641, F-33600 Pessac, France*²*CNRS, CRPP, UPR 8641, F-33600 Pessac, France*³*Univ. Bordeaux, IMB, UMR 5251, F-33400 Talence, France*⁴*INRIA, F-33400 Talence, France*⁵*Bordeaux INP, IMB, UMR 5251, F-33400 Talence, France*

(Received 2 August 2017; revised manuscript received 28 November 2017; published 22 December 2017)

The topology and creation energy of domain walls in different magnetic chains (called Single-Chain Magnets or SCMs) are discussed. As these domain walls, that can be seen as “defects”, are known to control both static and dynamic properties of these one-dimensional systems, their study and understanding are necessary first steps before a deeper discussion of the SCM properties at finite temperature. The starting point of the paper is the simple regular ferromagnetic chain for which the characteristics of the domain walls are well known. Then two cases will be discussed (i) the “mixed chains” in which isotropic and anisotropic classical spins alternate, and (ii) the so-called “canted chains” where two different easy axis directions are present. In particular, we show that “strictly narrow” domain walls no longer exist in these more complex cases, while a cascade of phase transitions is found for canted chains as the canting angle approaches 45° . The consequence for thermodynamic properties is briefly discussed in the last part of the paper.

DOI: [10.1103/PhysRevB.96.214429](https://doi.org/10.1103/PhysRevB.96.214429)**I. INTRODUCTION**

Single-chain magnets (SCMs) are one-dimensional (1D) molecule-based systems well known to exhibit slow relaxation of their magnetization [1]. For this reason, they are potential candidates for information storage and they have been intensively studied since their discovery in the beginning of the 2000s [2,3]. In these systems, the dynamic properties are explained by the conjugated effect of the magnetic anisotropy of chain repeating units and of the magnetic interactions between these units. As a result, these 1D systems only exhibit short-range magnetic order at low enough temperature. The corresponding equilibrium state of a chain consists of large magnetic domains separated by narrow domain walls (DWs), which are nonlinear excitations of the chain at $T = 0$. DWs, or more often called π solitons [4,5], are spontaneously created at finite temperature. Although they compete with other spin excitations [6,7], they play a crucial role in statistical mechanics (i.e., equilibrium properties) [8–10] as well as for dynamic properties of classical anisotropic ferromagnetic chains [11,12].

In these simple chains, all the magnetic units have the same anisotropy axis direction as well as a unique ferromagnetic exchange interaction between them. The size and shape of the DWs along these chains are then the key ingredients to understand their thermodynamic properties as well as the slow relaxation of their magnetization. A pioneering work to discuss the shape and energy of the DWs in a classical ferromagnetic chain has been already published by Barbara [13,14]. However, many SCMs present more complicated chain geometries. For example, some chains are built with an alternation of anisotropic and isotropic spins [15–24], called “mixed chains.” In many other systems, two different orientations of the

anisotropy axes alternate along the chain. These systems are usually labeled as “canted chains” [25–37]. In a previous work, we have shown that a canted chain with a specific canting angle of 45° is expected to have a singular behavior with $\pi/2$ DWs (instead of π DWs for the ferromagnetic chain) thus exhibiting a tetrastability and therefore would be a good candidate for four-bits-information storage [38]. In the present paper, we will focus on the description of the DW characteristics, namely their profile and their creation energy, in order to understand the static and dynamic properties of SCMs.

In a first part of this paper, the main results for the textbook ferromagnetic chain will be summarized together with a brief description of the numerical technique used to estimate the characteristics of the DWs. The following parts will be devoted to the mixed chains and then to the case of the canted chains for any value of the canting angle. The crossover towards the 45° canted chain will be also specifically discussed. Finally, concluding remarks will be given in the last part of the paper, in particular to discuss the implication of our results on the thermodynamic SCM properties at finite temperature.

II. REGULAR FERROMAGNETIC CHAIN

In this section, main characteristics of the regular ferromagnetic chain are summarized. Some of these results have already been obtained by Barbara [13,14]. This simple case will also be used to check the validity of our numerical method applied to more complicated chains as described in the following sections.

The structure of the regular ferromagnetic chain is depicted in Fig. 1. At $T = 0$, two equivalent equilibrium states coexist; see Figs. 1(a) and 1(b). A DW represents a spin configuration that links these two equivalent solutions [Fig. 1(c)]. In this case, the spin orientation varies from 0 to 180° and these DWs are therefore labeled as π DWs.

For a quantitative analysis, the starting Hamiltonian is the anisotropic Heisenberg Hamiltonian, given in Eq. (1) with

*Corresponding author: vivien.pianet@u-bordeaux.fr†coulon@crpp-bordeaux.cnrs.fr

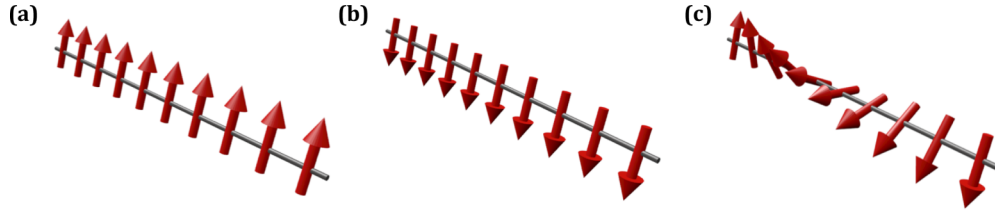


FIG. 1. Panels (a) and (b) show the two equivalent ground states of the chain at $T = 0$ K; (c) chain with a domain wall connecting the two equivalent ground states.

classical anisotropic spins:

$$H_{HA} = -2JS^2 \sum_{n=-\infty}^{+\infty} \vec{u}_n \cdot \vec{u}_{n+1} - DS^2 \sum_{n=-\infty}^{+\infty} u_{n,z}^2. \quad (1)$$

The first term describes the exchange energy (assuming only the first-neighbor interaction) with $J > 0$ in the ferromagnetic case, while the second part of Eq. (1) is the anisotropy term (\vec{u}_n is the unitary vector for the spin n). Considering a uniaxial anisotropy, the presence of an easy axis z implies $D > 0$. Introducing θ_n , the angle between the spin n and the z axis, the energy of the chain deduced from Eq. (1) is given by Eq. (2),

$$E = -2JS^2 \sum_{n=-\infty}^{+\infty} \cos(\theta_n - \theta_{n+1}) + DS^2 \sum_{n=-\infty}^{+\infty} \sin^2(\theta_n). \quad (2)$$

The energy of a DW [Eq. (3)] is obtained from Eq. (2) after removing the contribution of the chain without defect,

$$\frac{\Delta E}{2JS^2} = \sum_{n=-\infty}^{+\infty} [1 - \cos(\theta_n - \theta_{n+1})] + \frac{D}{2J} \sum_{n=-\infty}^{+\infty} \sin^2(\theta_n). \quad (3)$$

The profile of the DW is obtained by minimization of this energy with respect to the spin angles. This implies solving the set of Eqs. (4), in order to determine $\bar{\theta}_n$, the equilibrium value for each θ_n ,

$$\begin{aligned} \frac{\partial \Delta E}{\partial \theta_n} &= \sin(\bar{\theta}_n - \bar{\theta}_{n+1}) + \sin(\bar{\theta}_n - \bar{\theta}_{n-1}) \\ &+ \frac{D}{2J} \sin(2\bar{\theta}_n) = 0. \end{aligned} \quad (4)$$

The chosen boundary conditions are respectively $\bar{\theta}_i = 180^\circ$ and $\bar{\theta}_f = 0^\circ$ on the left and right chain ends. The DW characteristics result from the competition between the two terms in Eq. (2). As a consequence, their static properties only depend on the D/J ratio. There are therefore two simple limits for $D \gg J$ and $D \ll J$.

When the anisotropy is much larger than the exchange interaction, all the spins are close to their easy axis, i.e., $\bar{\theta}_n$ is either close to 0 or to 180° . The DW profile is narrow and symmetric relative to its center located between two consecutive spins. Its position can be defined as $n = -1/2$ between the spin $n = -1$ and $n = 0$, leading to the angular relation: $\bar{\theta}_{-n-1} = \pi - \bar{\theta}_n$ [13,14]. For positive values of n , where the equilibrium angles are small, the linearization of

Eq. (4) gives Eq. (5):

$$2\left(1 + \frac{D}{2J}\right)\bar{\theta}_n = \bar{\theta}_{n-1} + \bar{\theta}_{n+1}. \quad (5)$$

The solution of Eq. (5) is an exponential profile [Eq. (6)].

$$\bar{\theta}_n = \theta_0 e^{-n\psi}, \quad \text{with } \cosh(\psi) = (D/2J) + 1. \quad (6)$$

In order to fully describe the DW profile $\bar{\theta}_0$, the equilibrium value of θ_0 must be determined. Assuming a small value of the orientation angles and the exponential profile Eq. (6), the energy of the DW given by Eq. (3) can be developed up to the fourth order as shown by Eq. (7) (details are given in Appendix A):

$$\frac{\Delta E_{D \gg J}}{4JS^2} = 1 + \frac{(e^\psi - 3)}{2}\theta_0^2 + \frac{1}{10}\theta_0^4. \quad (7)$$

It is worth noting that Eq. (7) is reminiscent of a Landau development close to a second-order phase transition [39]. The equilibrium value $\bar{\theta}_0$ is obtained by minimizing this expression. When $D/J > 4/3$ (i.e. $\psi > \ln(3)$), the minimum value is zero, indicating that “strictly narrow domain walls” are found for any value of D/J above $4/3$. The spin orientation is either 180° or 0° and the width of the DW is only one unit cell. On the other hand, a broader profile, with the DW spread over several unit cells, is found below the critical value $D/J = 4/3$. Close to this critical point, minimizing Eq. (7) gives the approximate expression of $\bar{\theta}_0$ [Eq. (8)],

$$\bar{\theta}_0 = \sqrt{\frac{5(3 - e^\psi)}{2}}. \quad (8)$$

This expression of $\bar{\theta}_0$ is similar to the one obtained for a second-order phase transition treated in the frame of the mean-field approximation (here a classical model at $T = 0$ K is discussed and fluctuations are not expected). If this result is introduced in Eq. (7), a cusp of the DW energy is predicted at the critical point. Note that this energy remains constant and equal to $4JS^2$ above this point.

When the exchange energy is larger than the anisotropy, the first term of Eq. (2) dominates and is minimum when the orientation of two neighboring spins is very close. As a consequence, the DWs are broad and contain a finite number of unit cells. In order to determine the DW profile and energy, Eqs. (4) can be simplified into Eqs. (9):

$$2\bar{\theta}_n - \bar{\theta}_{n+1} - \bar{\theta}_{n-1} + \frac{D}{2J} \sin(2\bar{\theta}_n) = 0. \quad (9)$$

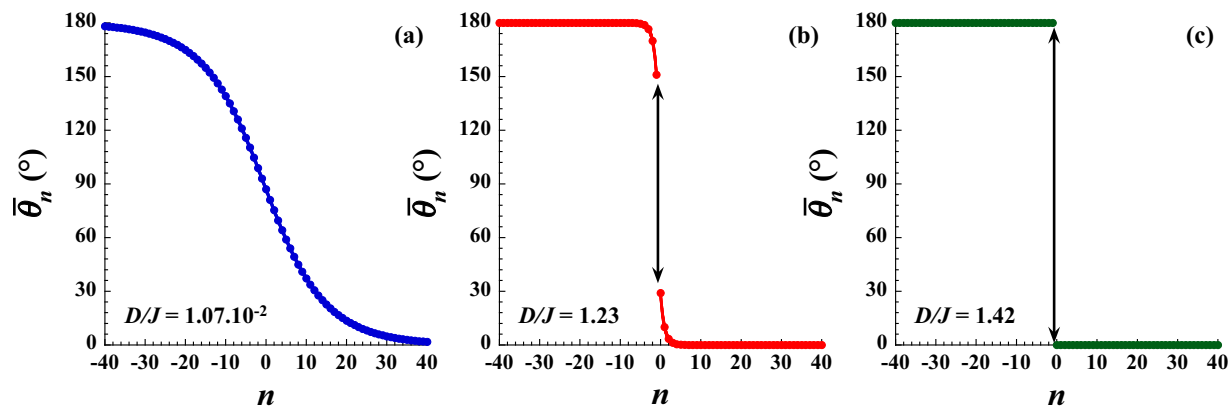


FIG. 2. DW profile obtained numerically for the ferromagnetic chain: (a) when D/J is small; (b) D/J close to or slightly smaller than $4/3$; (c) $D/J > 4/3$. The colored lines are the parametrizations of the numerical profiles by their analytic expressions Eqs. (11) and (6). As the DW center is located at $n = -1/2$, the right part of the profile begins with the spin labeled $n = 0$.

Considering the orientation angle as a continuous function of n , Eq. (9) becomes

$$\frac{d^2\bar{\theta}}{dn^2} = \frac{D}{2J} \sin(2\bar{\theta}). \quad (10)$$

A double integration of Eq. (10) gives Eq. (11) and thus the DW profile in this limit ($D \ll J$),

$$\tan\left(\frac{\bar{\theta}}{2}\right) = e^{-n\sqrt{\frac{D}{J}}}. \quad (11)$$

The corresponding DW energy can be estimated from Eq. (3) at the continuous approximation [Eq. (12)].

$$\frac{\overline{\Delta E}}{2JS^2} = \frac{1}{2} \int \left(\frac{d\bar{\theta}}{dn}\right)^2 dn + \frac{D}{2J} \int \sin^2(\bar{\theta}) dn, \quad (12)$$

and in the $D \ll J$ limit,

$$\frac{\overline{\Delta E}_{D \ll J}}{4JS^2} = \sqrt{\frac{D}{J}}. \quad (13)$$

In the general case between the two above limits, numerical calculations are necessary [40]. The resolution of Eqs. (4) can be performed using an iterative Newton-Raphson method (details are given in Appendix B). With this numerical approach, the DW profile and its corresponding energy can be determined for any D/J value. Typical profiles are given in

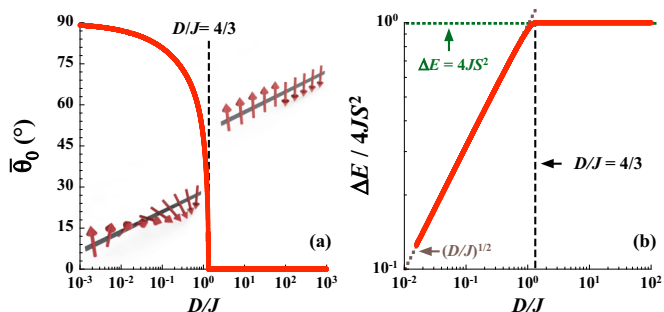


FIG. 3. (a) Orientation angle of the first spin after the DW center ($n = 0$) as a function of D/J for the ferromagnetic chain, and (b) the corresponding normalized energy.

Fig. 2. An excellent agreement is found between the numerical result and the profile given by Eq. (11) in Fig. 2(a) or by Eq. (6) in Figs. 2(b) and 2(c) close to the critical value of $D/J = 4/3$. As expected, a strictly narrow DW is found in the last case while the DW is spread over a few unit cells in Fig. 2(b). To illustrate the type of DW stabilized depending on D/J , Fig. 3(a) gives the orientation of the first spin of the DW right part ($n = 0$) as a function of D/J . Our numerical data are consistent with the scaling law [Eq. (8)] obtained close to the critical point. Finally, Fig. 3(b) gives the normalized energy of the DW as a function of D/J . The two extreme regimes together with the crossover at $D/J = 4/3$ are clearly visible.

III. “MIXED CHAIN” CASE

In this paper and as illustrated by Fig. 4, a “mixed chain” refers to a chain composed of an alternation of anisotropic classical spins S and isotropic spins s (not necessarily classical). Experimental examples of such chains are known [15–24], in particular, when the isotropic spin is a radical. Interactions between s and S are in most of the cases antiferromagnetic ($J < 0$) and thus this common situation will be considered in the following. The Fig. 4 illustrates two unit cells to describe this type of chain, each comprising one spin of each kind, associated to the different orientation angles (θ_n and κ_n).

In the following, we will consider the spins s as classical, the particular case of quantum spins being described in Appendix C. Starting from the anisotropic Heisenberg

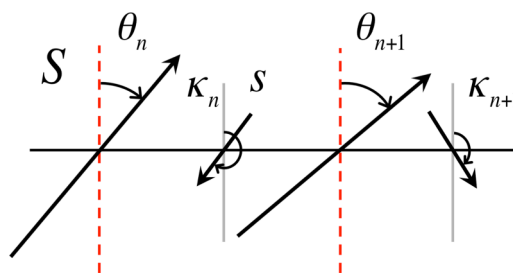


FIG. 4. Scheme and labeling of the spins and angles along the mixed chain.

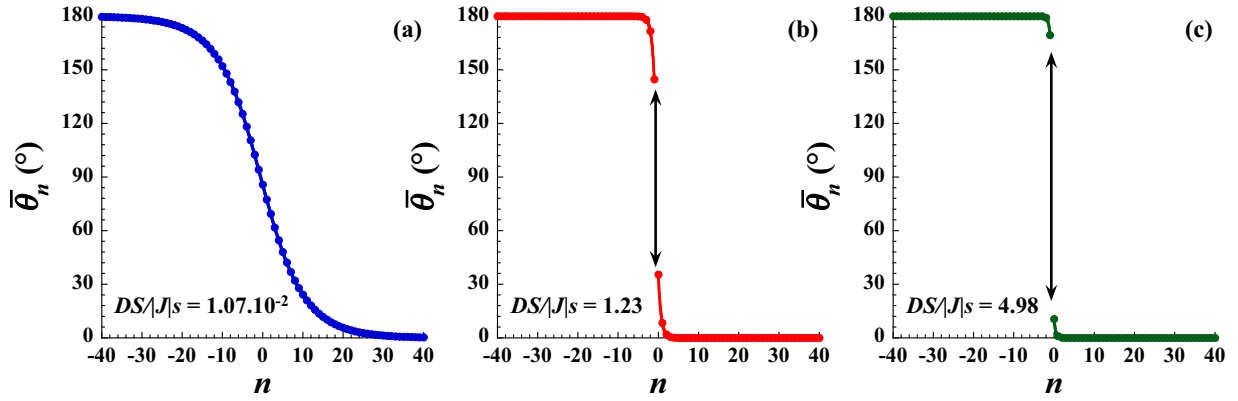


FIG. 5. DW profile for the mixed chain when (a) $DS/|J|s$ is small, (b) $DS/|J|s$ is close to 1; (c) $DS/|J|s$ is large. The colored lines are the parametrizations of the numerical profiles by their analytic expressions Eqs. (25) and (20).

Hamiltonian, the chain energy is given by Eq. (14),

$$E = 2|J|Ss \sum_{n=-\infty}^{+\infty} [\cos(\theta_n - \kappa_n) + \cos(\kappa_n - \theta_{n+1})] + DS^2 \sum_{n=-\infty}^{+\infty} \sin^2(\theta_n). \quad (14)$$

The minimization of this energy with respect to the orientation of the isotropic spins gives an angular relation [Eq. (15)] between the adjacent spins,

$$\bar{\kappa}_n = \frac{\theta_n + \theta_{n+1}}{2} + \pi. \quad (15)$$

Substitution of Eq. (15) into Eq. (14) gives an effective energy [Eq. (16)], which depends only on the orientations of the anisotropic spins,

$$\bar{E} = -4|J|Ss \sum_{n=-\infty}^{+\infty} \cos\left(\frac{\theta_n - \theta_{n+1}}{2}\right) + DS^2 \sum_{n=-\infty}^{+\infty} \sin^2(\theta_n). \quad (16)$$

Remarkably, the same expression is obtained if the isotropic quantum spins are considered (see Appendix C) or if the interactions between s and S spins are assumed to be ferromagnetic.

The normalized energy of a domain wall is given by Eq. (17) considering the difference between the chain energy [Eq. (16)] and the energy of the chain without DW. The minimization of Eq. (17) leads to a series of equations [Eqs. (18)] establishing the angular relation between neighboring spins,

$$\frac{\Delta \bar{E}}{4|J|Ss} = \sum_{n=-\infty}^{+\infty} \left[1 - \cos\left(\frac{\theta_n - \theta_{n+1}}{2}\right) \right] + \frac{DS}{4|J|s} \sum_{n=-\infty}^{+\infty} \sin^2(\theta_n), \quad (17)$$

$$\frac{\partial \bar{E}}{\partial \theta_n} = \sin\left(\frac{\bar{\theta}_n - \bar{\theta}_{n+1}}{2}\right) + \sin\left(\frac{\bar{\theta}_n - \bar{\theta}_{n-1}}{2}\right) + \frac{DS}{2|J|s} \sin(2\bar{\theta}_n) = 0. \quad (18)$$

As discussed in the ferromagnetic chain case, these relations [Eqs. (17) and (18)] can be simplified in the different limits.

In the narrow DW limit ($DS \gg |J|s$), the orientation angles for the right part of the DW are small and a linearization of Eq. (18) is possible as shown by Eq. (19):

$$2\left(1 + \frac{DS}{|J|s}\right)\bar{\theta}_n = \bar{\theta}_{n-1} + \bar{\theta}_{n+1}. \quad (19)$$

Again in this case, this equation can be solved by an exponential profile [Eq. (20)],

$$\bar{\theta}_n = \theta_0 e^{-n\psi}, \quad \text{with } \cosh(\psi) = DS/|J|s + 1. \quad (20)$$

As in the previous section, the full determination of the profile is obtained from a development of Eq. (17). After introducing the exponential profile [Eq. (20)] an expression of $\Delta \bar{E}$ depending only on θ_0 is obtained [Eq. (21)],

$$\frac{\Delta \bar{E}_{D \gg |J|}}{4|J|Ss} = 1 - \theta_0 + \left(\frac{e^\psi - 1}{2}\right) \frac{\theta_0^2}{2}. \quad (21)$$

The minimization of Eq. (21) gives an approximation of the equilibrium value of θ_0 [Eq. (22)],

$$\bar{\theta}_0 = \frac{2}{e^\psi - 1}. \quad (22)$$

This result underlines that $\bar{\theta}_0$ is always finite, i.e., has a nonzero value, for any positive value of $D/|J|$ since ψ remains in this case strictly positive. This implies that strictly narrow DWs no longer exist. Moreover, the coefficient of the quadratic term in Eq. (21) remains positive for any positive value of $D/|J|$ which means that the critical point found for the regular chain is pushed at $D/|J| = 0$ (i.e., for $\psi = 0$).

In the broad DW limit ($DS \ll |J|s$), as in the previous section, Eqs. (23) take advantage of the small variation of the orientation angles with n to simplify Eqs. (18) and in the continuous limit Eq. (24) is obtained:

$$\bar{\theta}_n - \frac{\bar{\theta}_{n+1} + \bar{\theta}_{n-1}}{2} + \frac{DS}{2|J|s} \sin(2\bar{\theta}_n) = 0, \quad (23)$$

$$\frac{d^2 \bar{\theta}}{dn^2} = \frac{DS}{|J|s} \sin(2\bar{\theta}). \quad (24)$$

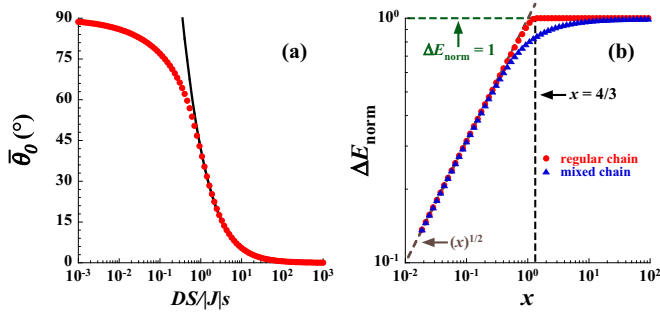


FIG. 6. (a) Orientation of the first spin after the DW center as a function of $DS/|J|s$ for the mixed chain. The black line is the analytical expression of $\bar{\theta}_0$ given by Eq. (22) in the $DS \gg |J|s$ limit; (b) corresponding normalized energy (the comparison is made with the regular ferromagnetic chain). x is $DS/2|J|s$ or D/J for the mixed or regular chain cases respectively. ΔE_{norm} is $\Delta \bar{E}/4|J|Ss$ or $\Delta E/4JS^2$ for the mixed or regular chain systems respectively.

Double integration of Eq. (24) gives Eq. (25) and the DW profile in the ($DS \ll |J|s$) limit,

$$\tan\left(\frac{\bar{\theta}}{2}\right) = e^{-n\sqrt{2DS/|J|s}}. \quad (25)$$

The corresponding DW energy, Eq. (26), can also be deduced from Eq. (17) at the continuous approximation.

$$\frac{\overline{\Delta \bar{E}}}{4|J|Ss} = \frac{1}{8} \int \left(\frac{d\bar{\theta}}{du}\right)^2 dn + \frac{DS}{4|J|s} \int \sin^2(\bar{\theta}) dn \quad (26)$$

In the broad DW limit, Eq. (26) simplifies to Eq. (27),

$$\overline{\Delta \bar{E}}_{DS \ll |J|s} = 4Ss \sqrt{\frac{D|J|S}{2s}}. \quad (27)$$

It worth noticing that the scaling law in $\sqrt{D|J|}$ of the DW energy of the regular ferromagnetic chain in the broad DW limit is preserved in the mixed case.

In the general case, the numerical approach is the only one accessible. As for the regular chain, the DW profile can be deduced for any value of $DS/|J|s$. Typical results are given in Fig. 5, in the broad [Fig. 5(a)] and narrow [Figs. 5(b) and 5(c)] DW limits.

When $DS/|J|s$ is small [Fig. 5(a)], an excellent agreement is found between the numerical result and the profile given by Eq. (25). As expected, a strictly narrow DW (i.e., on one site) is never found when $DS \gg |J|s$ as shown in Fig. 5(c). This is also illustrated by Fig. 6(a) which gives the evolution

of the $n = 0$ spin orientation as a function of $DS/|J|s$. These numerical data are consistent with the analytical expression obtained when $DS \gg |J|s$ [Eq. (22), Fig. 6(a)]. The absence of critical point in the mixed chain case is clearly established when the normalized energy of the DW is plotted as a function of $DS/|J|s$ and compared with the analogous energy found in the ferromagnetic regular chain case (*vide supra*) as shown in Fig. 6(b).

IV. CANTED CHAIN CASE

In the present work, a canted chain refers to a 1D spin system with at least two different orientations of the easy axis along the chain [41]. The case of two different orientations is commonly realized experimentally and is thus the focus of the following discussion with spin and angle definitions given in Fig. 7.

In a previous paper [38], the specific case where $\alpha = 45^\circ$ was analyzed in great detail, showing that $\pi/2$ DWs are found instead of the regular π DWs (see Sec. I). In this section, this theoretical approach is generalized for any canting angle comprised between 0 and 45° . Starting from the ferromagnetic solution [Eq. (2)] and taking into account a canting angle, the chain energy is given by Eq. (28):

$$E = -2JS^2 \sum_{n=-\infty}^{+\infty} [\cos(\phi_n - \theta_n) + \cos(\theta_n - \phi_{n+1})] + DS^2 \sum_{n=-\infty}^{+\infty} [\sin^2(\phi_n + \alpha) + \sin^2(\theta_n - \alpha)]. \quad (28)$$

Minimization of this energy gives two sets of equations [Eqs. (29)],

$$\begin{aligned} \frac{\partial \bar{E}}{\partial \theta_n} &= \sin(\bar{\theta}_n - \bar{\phi}_n) + \sin(\bar{\theta}_n - \bar{\phi}_{n+1}) \\ &+ \frac{D}{2J} \sin(2\bar{\theta}_n - 2\alpha) = 0, \\ \frac{\partial \bar{E}}{\partial \phi_n} &= \sin(\bar{\phi}_n - \bar{\theta}_n) + \sin(\bar{\phi}_n - \bar{\theta}_{n-1}) \\ &+ \frac{D}{2J} \sin(2\bar{\phi}_n + 2\alpha) = 0. \end{aligned} \quad (29)$$

Equations (29) are used to estimate the equilibrium values of the orientation angles ($\bar{\theta}_n$ and $\bar{\phi}_n$) in the absence of DWs. In this case, the spin orientations are independent of n ($\bar{\theta}_n = \theta_e$ and $\bar{\phi}_n = \phi_e$). When introduced in Eqs. (29), only

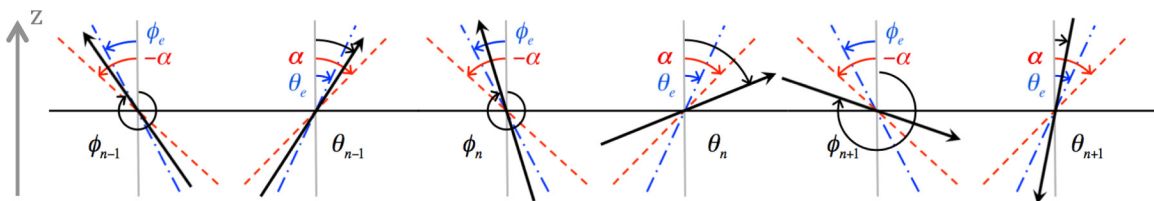


FIG. 7. Labeling the spins and angles for the canted chain. The red dashed lines and blue dot-dashed lines represent the two easy-axis orientations and the two equilibrium orientations respectively. The angle between the z axis and the easy axes are respectively $-\alpha$ and $+\alpha$ (the so-called canting angle is therefore 2α). The corresponding orientation angles will be labeled respectively ϕ_n and θ_n . As in the previous section, each unit cell contains one spin of each kind.

two absolute minima of the energy are found for any value of the canting angle smaller than 45° . The first solution corresponds to $\phi_e = -\theta_e$ with $0 < \theta_e < \alpha$. The second one is deduced adding 180° to each of the equilibrium angles. As for the ferromagnetic chain, the two domains corresponding to these two solutions will be connected by π DWs. Moreover, Eqs. (29) also imply Eqs. (30), which link θ_e , α , D , and J parameters:

$$\frac{\sin(2\theta_e)}{\sin(2\alpha - 2\theta_e)} = \frac{D}{4J} \text{ or } \tan(2\theta_e) = \frac{D}{4J} \frac{\sin(2\alpha)}{1 + \frac{D}{4J} \cos(2\alpha)}. \quad (30)$$

As in the previous sections, the energy of the DW is obtained subtracting the energy of the chain without DWs [Eq. (31)]. In the following, we will discuss the different DW profiles according to the value of D/J :

$$\frac{\Delta E}{2JS^2} = \sum_{n=-\infty}^{+\infty} [2 \cos(2\theta_e) - \cos(\phi_n - \theta_n) - \cos(\theta_n - \phi_{n+1})] + \frac{D}{2J} \sum_{n=-\infty}^{+\infty} [\sin^2(\phi_n + \alpha) + \sin^2(\theta_n - \alpha) - 2\sin^2(\theta_e - \alpha)]. \quad (31)$$

In the case of narrow DWs ($D \gg J$), Eq. (31) can be linearized [Eqs. (32)] with small angular variables, $\delta\bar{\theta}_n$ and $\delta\bar{\phi}_n$, obtained by considering the deviation from the equilibrium angles θ_e and ϕ_e ($\phi_e = -\theta_e$): $\delta\bar{\theta}_n = \bar{\theta}_n - \theta_e$ and $\delta\bar{\phi}_n = \bar{\phi}_n + \theta_e$,

$$\left[\frac{D \cos(2\theta_e - 2\alpha)}{J \cos(2\theta_e)} + 2 \right] \delta\bar{\theta}_n = \delta\bar{\phi}_n + \delta\bar{\phi}_{n+1}, \quad \left[\frac{D \cos(2\theta_e - 2\alpha)}{J \cos(2\theta_e)} + 2 \right] \delta\bar{\phi}_n = \delta\bar{\theta}_n + \delta\bar{\theta}_{n-1}. \quad (32)$$

As for the ferromagnetic chain case, an exponential DW profile [Eqs. (33)] is found (the center of the DW being between ϕ_0 and θ_0):

$$\begin{aligned} \delta\bar{\theta}_n &= \delta\theta_0 e^{-n\psi'} & \text{for } n \geq 0 \\ \delta\bar{\phi}_n &= \delta\theta_0 e^{-(n-\frac{1}{2})\psi'} & \text{for } n \geq 1 \end{aligned} \quad \text{with } \cosh\left(\frac{\psi'}{2}\right) = \frac{D \cos(2\theta_e - 2\alpha)}{2J \cos(2\theta_e)} + 1. \quad (33)$$

This result [Eqs. (33)] is a generalization of Eq. (6) which corresponds to the case $\alpha = 0^\circ$ and $\psi' = 2\psi$ (reflecting the fact that the chain unit cell contains two spins in the canted case). This exponential profile can be introduced in Eq. (31) to obtain an effective energy [Eq. (34)] only dependent on $\delta\theta_0$ up to the second order,

$$\frac{\overline{\Delta E}}{4JS^2} = \cos(2\theta_e) \left[1 + \frac{e^{\psi'/2} - 3}{2} \delta\theta_0^2 \right] - 2 \sin(2\theta_e) \delta\theta_0. \quad (34)$$

Again, as in the ferromagnetic case, the coefficient of the quadratic term vanishes at a finite value of D/J corresponding to $\exp(\psi'/2) = 3$. This result is reminiscent of the critical point found for the ferromagnetic case. However, the last term of Eq. (34) implies that $\sin(2\theta_e)$ acts as an external field linearly coupled to the order parameter $\delta\theta_0$. As shown by Eq. (30), this external field is finite as soon as the canting angle is nonzero. As a consequence, strictly narrow DWs do not exist in canted chains.

In order to calculate the energy of DWs, Eq. (34) was minimized to estimate $\delta\bar{\theta}_0$ (the equilibrium value of $\delta\theta_0$) in the narrow DW limit, for $\exp(\psi'/2) > 3$. Introducing $\delta\bar{\theta}_0$ in Eq. (34) then gives Eq. (35a) the corresponding creation energy of the DW.

$$\frac{\overline{\Delta E}_{D \gg J}}{4JS^2} = \cos(2\theta_e) \left[1 - \frac{2 \tan^2(2\theta_e)}{e^{\psi'/2} - 3} \right]. \quad (35a)$$

Using Eqs. (30) and (33), a simplified expression of Eq. (35a), valid when D/J is large and α close to 45° , is obtained [Eq. (35b)].

$$\frac{\overline{\Delta E}_{D \gg J}}{4JS^2} \approx \frac{2J}{D} + \cos(2\alpha) \quad (35b)$$

This energy expression shows a crossover between a linear law ($\overline{\Delta E}_{D \gg J}/4JS^2 \approx 2J/D$) and a saturation regime [$\overline{\Delta E}_{D \gg J}/4JS^2 \approx \cos(2\alpha)$] depending on the competition between two reduced parameters: J/D and $45 - \alpha$. Although the ‘‘Ising limit,’’ where the normalized energy becomes $\cos(2\alpha)$, is finally reached when D/J is large enough, it should be noticed that very large values of D/J are required to reach this limit when α is close to 45° . For example, in the case $\alpha = 44^\circ$, the crossover occurs for $D/J = 57$.

As in the previous section, the problem can be simplified in the broad DWs case ($D \ll J$), taking profit of the small variation of the orientation angles. The details of the calculation are given in Appendix D and the essential steps are summarized in the following paragraph.

In order to easily describe the DW’s profile, we introduce the variables, ω_n and γ_n [Eq. (36)]

$$\omega_n = \frac{\delta\phi_n + \delta\theta_n}{2}, \quad \gamma_n = \frac{\delta\phi_n - \delta\theta_n}{2}. \quad (36)$$

The energy of the DW [see Eq. (31)] can be developed [Eq. (37)] in power of the small parameters γ and $d\omega/dn$ (where ω and γ are the variables corresponding to ω_n and γ_n in the continuous limit),

$$\begin{aligned} \frac{\Delta E}{4JS^2 \cos(2\theta_e)} &= \int \left\{ \gamma^2 + \left(\frac{1}{2} \frac{d\omega}{dn} + \gamma \right)^2 \right\} dn \\ &+ 2 \sinh^2\left(\frac{\psi'}{4}\right) \int \{\sin^2 \omega\} dn \\ &- \tan(2\theta_e) \int \left\{ 4\gamma \sin^2 \omega + \frac{1}{2} \frac{d\omega}{dn} \right\} dn. \end{aligned} \quad (37)$$

Successive minimizations with respect to γ , first, and then to ω , gives Eq. (38) with $a = 4 \sinh(\psi'/4)$ and $\tan(2\theta_e) = ka/4$:

$$\frac{d^2\bar{\omega}}{dn^2} = \frac{a^2}{2} \sin(2\bar{\omega})[1 - 2k^2\sin^2(\bar{\omega})]. \quad (38)$$

An exact double integration of this equation is possible and gives $\bar{\omega}$ and $\bar{\gamma}$ [Eqs. (39)]:

$$\tan(\bar{\omega}) = \frac{1}{\sqrt{1-k^2}} \frac{1}{\sinh(an)}, \quad (39a)$$

$$\bar{\gamma} = \frac{a \cosh(an)\sqrt{1-k^2} + ka}{4[1 + (1-k^2)\sinh^2(an)]}. \quad (39b)$$

After a rather technical but straightforward calculation, the DW energy [Eq. (40)] is deduced introducing $\bar{\omega}$ and $\bar{\gamma}$ [Eqs. (39)] in Eq. (37):

$$\frac{\overline{\Delta E}}{4JS^2 \cos(2\theta_e)} = \frac{a}{4} F(k) \quad \text{with} \quad (40)$$

$$F(k) = 1 + \left(\frac{k^2 - 1}{2k} \right) \ln \left(\frac{1-k}{1+k} \right).$$

It is worth noting that the function $F(k)$, which varies between 1 and 2, acts as a simple numerical factor. For small D/J and α close to 45° , the parameter a can be approximated by Eq. (41), and thus Eq. (40) can be simplified as Eq. (42). Again, a crossover between two different regimes [omitting $F(k)$], namely $\overline{\Delta E}/4JS^2 \approx D/4J$, and $\overline{\Delta E}/4JS^2 \approx \sqrt{D} \cos(2\alpha)/J/2$, is identified depending on the competition between two small parameters D/J and $45 - \alpha$,

$$a \approx 2\sqrt{\frac{D}{J} \left(\frac{D}{4J} + \cos(2\alpha) \right)}, \quad (41)$$

$$\frac{\overline{\Delta E}}{4JS^2} \approx \frac{F(k)}{2} \sqrt{\frac{D}{J}} \sqrt{\cos(2\alpha) + \frac{D}{4J}}. \quad (42)$$

As in the previous cases, numerical calculations were performed to extrapolate between the above two limits.

Figure 8(a) gives examples of numerical DW profiles in the limit $D/J > 1$. These numerical results are in agreement with

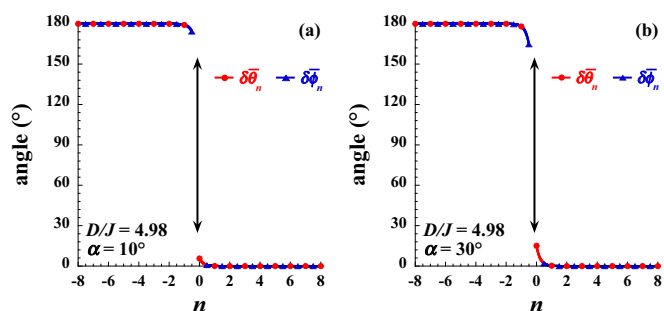


FIG. 8. DWs profiles for the canted chain for $D/J = 4.98$ with (a) a moderate canting angle, $\alpha = 10^\circ$, and with (b) a larger canting angle of 30° . Consistent with the unit cell (see Fig. 7), $\delta\bar{\phi}_n$ values are positioned at the abscisse $n + 1/2$ on the figures. The continuous lines give the parametrization of the numerical profile by the analytical expressions, Eqs. (33).

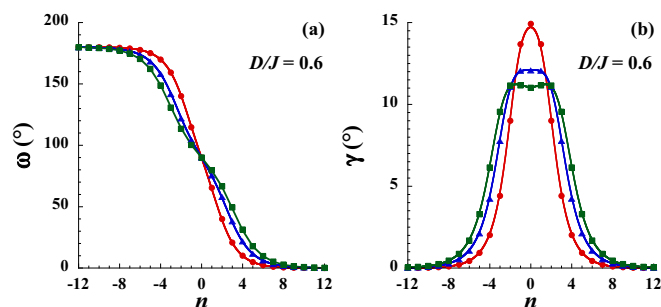


FIG. 9. Examples of DWs profiles for the canted chain with $D/J = 0.6$ and for α values of 42.78° (red circles), 44.29° (blue triangles), and 44.65° (green squares). The definition of the $\bar{\omega}$ (a) and $\bar{\gamma}$ (b) angles is given in the text. The continuous lines give the result of the analytical calculation [Eqs. (39)] without adjustable parameter.

the analytical conclusions, and confirm that strictly narrow DWs no longer exist when any finite value of the canting angle is introduced. At $D/J = 0.6$, which is already in the broad DW limit, the numerical DWs are shown in Fig. 9's profiles for selected α values. The continuous lines are fits using analytical equations [Eqs. (39)], which show a very good agreement with the numerical data. The evolution of $\delta\bar{\theta}_0$ as a function of D/J for different canting angles (Fig. 10) is also consistent with the analytical results obtained in the simple limits. This result emphasizes the fact that the canting angle simply induces an external field linearly coupled to the order parameter $\delta\bar{\theta}_0$.

The energy of the DWs as a function of D/J for different canting angles was also calculated as shown in Fig. 11. The two crossovers described analytically before are clearly seen in the $D \ll J$ and the $D \gg J$ limits when the canting angle approaches 45° .

The different equations deduced in the previous subsections are also consistent with the results obtained for the specific $\alpha = 45^\circ$ case [38]. For example, Eqs. (35b) and (42) give

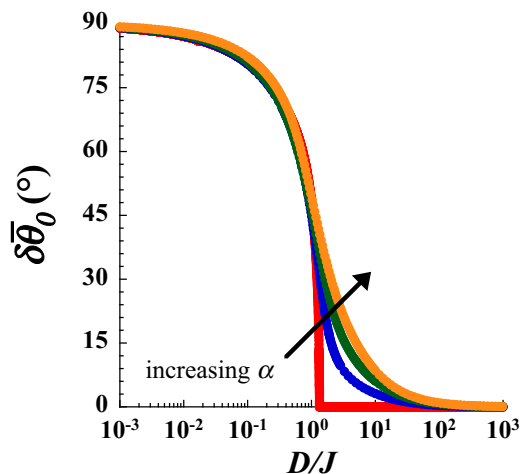


FIG. 10. Orientation of the first spin after the DW center as a function of D/J for a chain with different canting angles [$\alpha = 0$, in red, corresponding to the regular ferromagnetic chain, $\alpha = 10^\circ$ (blue), $\alpha = 20^\circ$ (green), and $\alpha = 30^\circ$ (orange)].

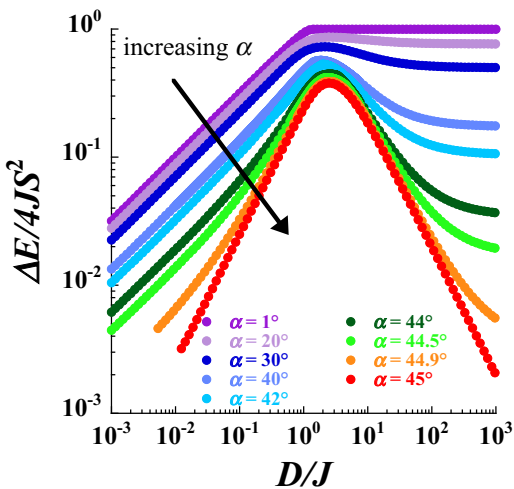


FIG. 11. Normalized creation energy of a domain wall for the canted chain considering several values of the canting angle from 1° to 45°. The comparison is also made with twice the creation energy of a $\pi/2$ DW in the singular $\alpha = 45^\circ$ case (see text).

the scaling laws deduced in this special limit. However, the energy of a DW is twice the one obtained for the $\alpha = 45^\circ$ case. Indeed, for any value of the canting angle smaller than 45° , π DWs are found in contrast to the $\pi/2$ DWs stabilized when the canting angle is exactly equal to 45° . Then, as done in Fig. 11, the energy for two $\pi/2$ DWs in the $\alpha = 45^\circ$ case should be compared with the one of a single π DW for smaller canting angles. Moreover, the different characteristics of the DWs mean that there is a qualitative difference between these cases. Therefore, the evolution of the DW’s profile while the canting angle approaches $\alpha = 45^\circ$ should be discussed in more detail. The following discussion mostly relies on numerical results, although some analytical results will be presented for comparison and verification of the limit cases.

Figure 12 that gives the evolution of the numerical profiles for $D/J = 4$ when the canting angle increases close to 45° is a good starting point. A careful examination of these DW profiles shows qualitative differences. In Fig. 12(a), the shape of the DW for $\alpha = 44^\circ$ is representative of the results obtained

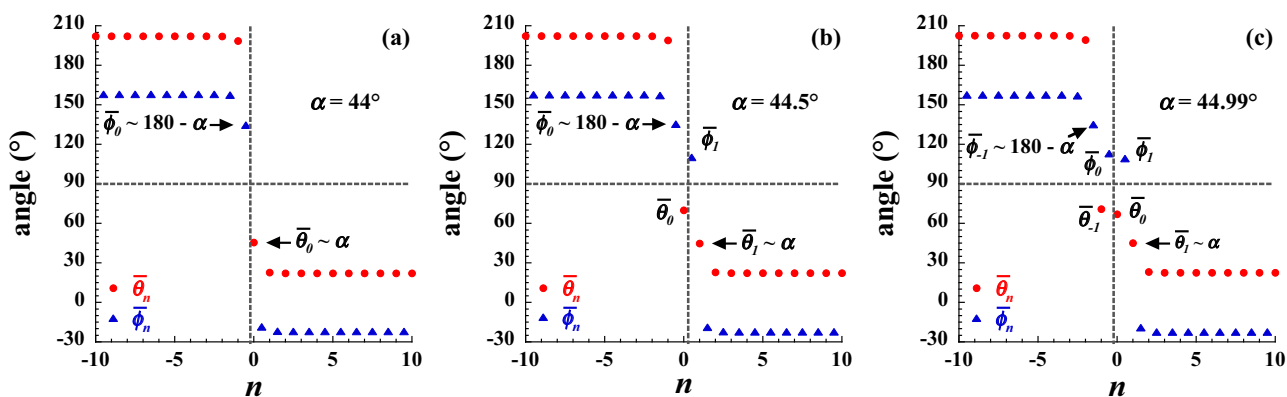


FIG. 12. Evolution of the DW profile as the canting angle approaches 45° for $D/J = 4$, i.e., in the large D/J limit. The parameter p defined in the text is 0, 1, and 2 for (a)–(c) respectively. Consistent with the unit cell (see Fig. 7), $\bar{\phi}_n$ values are positioned at the abscisse $n + 1/2$ on the figures.

for smaller canting angles. As D/J is large ($D/J = 4$ in the present case), the DW is narrow; i.e., the first spin after the DW center, θ_0 , is close to $180 - \alpha$, while the first spin before this center, ϕ_0 , is close to $180 - \alpha$. The situation is different for $\alpha = 44.5^\circ$ [Fig. 12(b)]. θ_0 is now located just before the DW center and the first spin after the DW center is ϕ_1 . It is now θ_1 which is close to α . The comparison between Figs. 12(a) and 12(b) shows clearly that a couple of spins have been introduced in the center of the DW profile for $\alpha = 44.5^\circ$. The size of this spin core further increases when the canting angle approaches 45° . For example, the core is composed of two couples of spins for $\alpha = 44.99^\circ$ as shown in Fig. 12(c). In the following, these different characteristic profiles will be labeled using a parameter p giving the number of couples of spins present in the central core of the DW. Thus, Figs. 12(a)–12(c) respectively correspond to $p = 0, 1$, and 2. It should be noted that profiles for odd and even p values are qualitatively different as the role of a θ and a ϕ spin are interchanged. Then, a phase transition occurs between $p = 0$ and $p = 1$, as between $p = 1$ and $p = 2$ or more generally between odd and even profiles. As a consequence, a cascade of phase transitions is observed as α approaches 45° . In the limit where p goes to infinity (as α goes to 45°), the core size increases as well and the profile becomes equivalent to two spatially separated $\pi/2$ DWs, in agreement with the situation already described when the canting angle is exactly equal to 45° [38].

The DW energy for different p values can be obtained by numerical calculations as shown in Fig. 13 for $D/J = 4$ comparing $p = 0, 1$, and 2 profiles. This figure illustrates, for large D/J values, that the $p = 0$ phase is stable until canting angles very close to 45° are reached. However, this result doesn’t hold when D/J is close to 1 for which the $p = 0/p = 1$ transition occurs for a canting angle close to 38° (*vide infra*).

Because of the qualitative difference between odd and even solutions, a cascade of phase transitions is still expected to exist for smaller D/J values. To illustrate this regime, Fig. 14 gives typical results obtained for $D/J = 0.2$. For $\alpha = 33$ or 40° [Figs. 14(a) and 14(c)], the first spin after the center of the DW is a “ θ ” one. In fact, these DW profiles correspond respectively to $p = 0$ and 2. On the other hand, the first spin after the center of the DW is a “ ϕ ” one for $\alpha = 36^\circ$ [Fig. 14(b)] corresponding

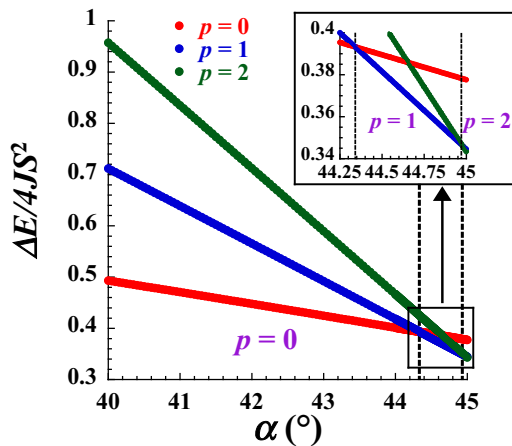


FIG. 13. Creation energy of a domain wall as a function of the canting angle for $D/J = 4$ to evidence the crossing between the different p solutions. The stable solution is also mentioned in purple at the bottom of the figure.

to $p = 1$. For this small D/J value, the existence of a spin core is less visible and it is useful to focus the discussion on the difference between even and odd solutions. The stable DW profile corresponds to $p = 0$ for small canting angles. At the introduced approximation, this calculation also describes other even values of p . To describe DW profiles with odd values of p , the role of θ and ϕ should be interchanged. In other words θ_e and k should be changed respectively into $-\theta_e$ and $-k$. Therefore, the generalized version of the DW energy in the $D \ll J$ limit [Eq. (37)] is now given by Eq. (43) (with $\varepsilon = 1$ or -1 for even or odd profiles respectively, and ω and γ being the reduced variable introduced earlier in Sec. III):

$$\begin{aligned} \frac{\Delta E}{4JS^2 \cos(2\theta_e)} = & \int \left\{ \gamma^2 + \left(\frac{1}{2} \frac{d\omega}{dn} + \gamma \right)^2 \right\} dn \\ & + 2 \sinh^2 \left(\frac{\psi'}{4} \right) \int \{ \sin^2 \omega \} dn \\ & - \varepsilon \tan(2\theta_e) \int \left\{ 4\gamma \sin^2 \omega + \frac{1}{2} \frac{d\omega}{dn} \right\} dn. \end{aligned} \quad (43)$$

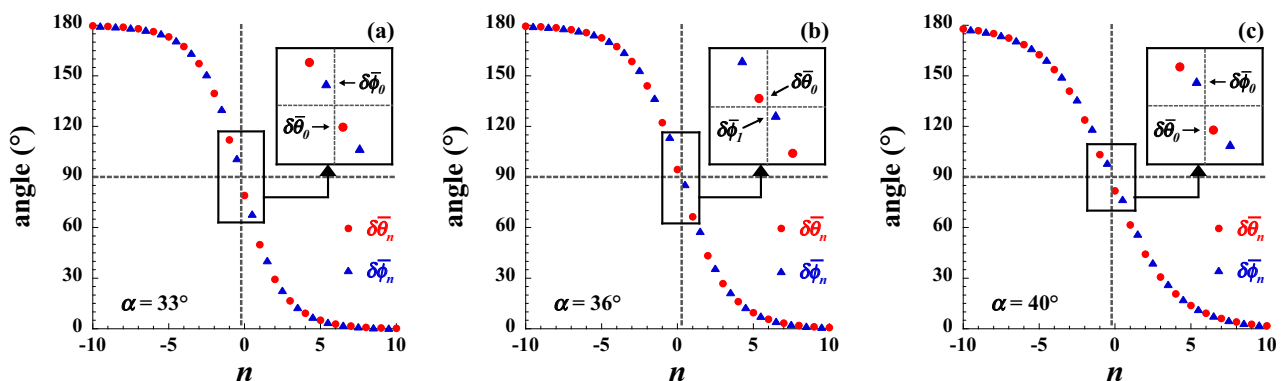


FIG. 14. Evolution of the DW profile as the canting angle approaches 45° for $D/J = 0.2$, i.e., in the small D/J limit. The parameter p defined in the text is 0, 1, and 2 for Figs. 14(a)–14(c) respectively. Consistent with the unit cell (see Fig. 7), $\delta\bar{\phi}_n$ values are positioned at the abscisse $n + 1/2$ on the figures.

Minimizing this expression [Eq. (43)] with respect to γ , an effective energy depending only on $\bar{\omega}$ is obtained [Eq. (44)]:

$$\begin{aligned} \frac{\Delta \tilde{E}}{4JS^2 \cos(2\theta_e)} = & \int \left(\frac{1}{8} \left(\frac{d\bar{\omega}}{dn} \right)^2 + \frac{a^2}{8} \sin^2(\bar{\omega}) [1 - k^2 \sin^2(\bar{\omega})] \right. \\ & \left. - \varepsilon \frac{ka}{4} \left(\frac{1}{2} - \sin^2(\bar{\omega}) \right) \frac{d\bar{\omega}}{dn} \right) dn. \end{aligned} \quad (44)$$

However, since the last term in this integral does not give any contribution to the energy, the equilibrium energy is independent of ε at this approximation. The minimization of the first two terms in Eq. (44) gives the same expression of $\bar{\omega}$ for $\varepsilon = 1$ or -1 , and is still given by Eq. (39a). On the other hand, the expression of $\bar{\gamma}$ [Eq. (39b)] should be generalized leading to Eq. (45):

$$\bar{\gamma} = \frac{a \cosh(an) \sqrt{1 - k^2} + \varepsilon ka}{4[1 + (1 - k^2) \sinh^2(an)]}. \quad (45)$$

In this case, numerical results can be used again to probe the accuracy of this analytical profile (see Fig. 15). The comparison of the results at $D/J = 0.6$, shown in Figs. 9 and 15, highlights that increasing α gives an alternation of even and odd profiles, both of them being consistent with Eqs. (39) and (45). The same conclusion is true for other values of D/J in the broad DW limit. Note that the fit with Eq. (45) becomes better as α approaches 45° probably because D/J is not small enough or because the profile is not exactly the one given by the analytical approach when k is too small (see Appendix E).

Besides the determination of the profiles, the numerical calculations also give the energy of the DWs. Consistent with a cascade of phase transitions when increasing α for a given value of D/J , even and odd profiles have alternatively the lowest energy. In other words, although very small, a finite-energy difference exists between even and odd profiles while this energy difference vanishes when a phase transition occurs between two successive p values. This finding is well illustrated by Fig. 16 where the absolute value of this difference is shown on a log scale.

Returning to Eq. (44), the result of the integral being independent of ε as the last term does not contribute, even

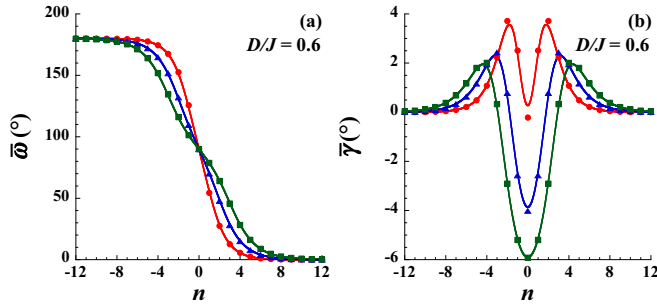


FIG. 15. Additional examples of DW profiles for the canted chain with $D/J = 0.6$ and for α values of 40.78° (red circles), 43.76° (blue triangles), and 44.59° (green squares). The definition of $\bar{\omega}$ and $\bar{\gamma}$ are given in the text. The continuous lines give the result of the analytical calculation [Eqs. (39a) and (45) with no adjustable parameter]. For these values of the canting angle, odd values of p correspond to the stable solution ($p = 1, 3, 5$ respectively as α increases for the selected data).

and odd profiles have always the same energy and hence this calculation does not lift the degeneracy between the two kinds of DW profiles. However, the starting expression of the energy [Eq. (31)] relies on a discrete sum rather than an integral. The small difference between the two formulations is the key to understanding the cascade of phase transitions in the small D/J limit. This argument is developed in Appendix E where the discrete sum for the last term of Eq. (44) is estimated from the analytical profile. The calculation predicts the existence of a master curve when reduced variables, $x = \pi\lambda/a$ and $y = (\Delta E_{1,-1}/4JS^2)e^{\pi^2/a}$ with $\lambda = \ln[(1+k)/(1-k)]$, are used. Numerical results confirm this finding as shown by Fig. 17. Remarkably, the analytical results [Eq. (E11)] even quantitatively reproduce the numerical data in the simple limit where $k \gg a$ (or $x \gg 2\pi$ when D/J is small; see Appendix E). To follow the numerical results for smaller k

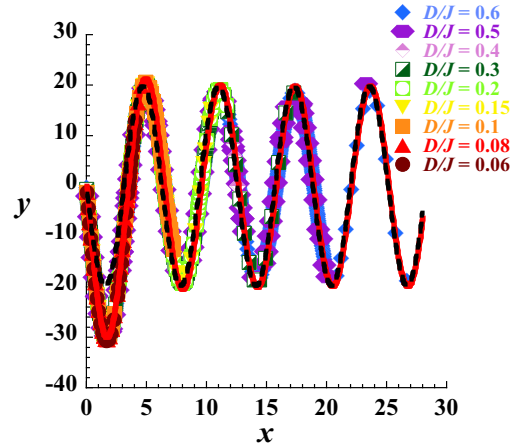


FIG. 17. Master curve plot deduced from numerical data introducing the reduced variables defined in Appendix E. The black dashed and red continuous curves correspond respectively to the simple expression obtained analytically [Eq. (E11)] [$y = -2\pi^2 \sin(x)$] and to the empirical expression [Eq. (E12)] given in Appendix E. The simple expression is in fact an excellent approximation when $x \gg 2\pi$.

values, an empirical expression [Eq. (E12)] has been used (see Appendix E). This allows an extrapolation of the numerical results when D/J goes to zero. The whole set of data summarizing the deduced phase diagram is given in Fig. 18 with a zoom in Fig. 19 to show the extrapolation for $D/J = 0$. The labeling of the different phases is given by specifying the p parameter. Finally, it should be noted that the energy difference between even and odd solutions, proportional to $\exp(-\pi^2/a)$, becomes very small for small D/J values. Then, the energy given in Fig. 11 remains an excellent approximation to estimate the DW energy in the broad DW limit.

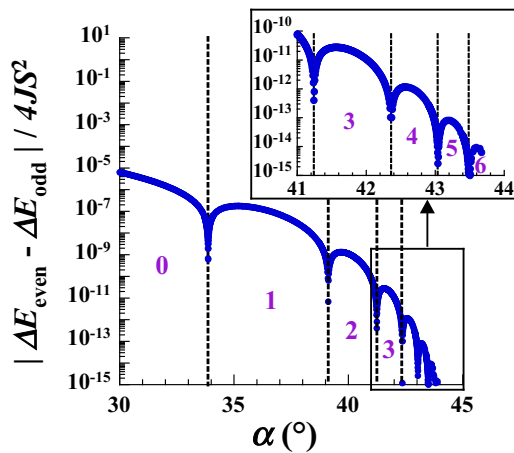


FIG. 16. Normalized absolute value of the creation energy difference between even and odd solutions as a function of the canting angle for $D/J = 0.2$. The p value of the stable solution is also given in purple.

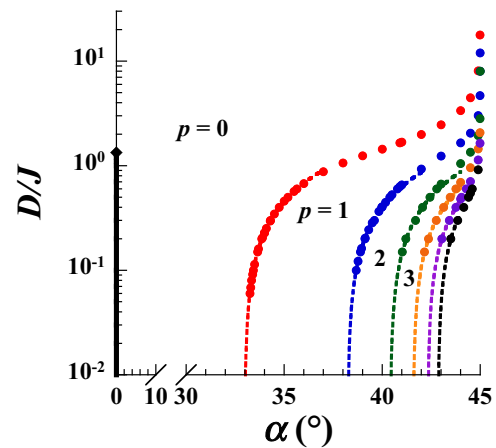


FIG. 18. Phase diagram for the canted spin chain case. The dots correspond to points on the transition lines that are extracted from numerical calculations. The extrapolation to $D/J = 0$ is given by the dashed lines. The different p values for the stable solution are also given. The black line recalls the existence of second-order phase transition which ends with the critical point (black dot) for $\alpha = 0$ and $D/J = 4/3$.

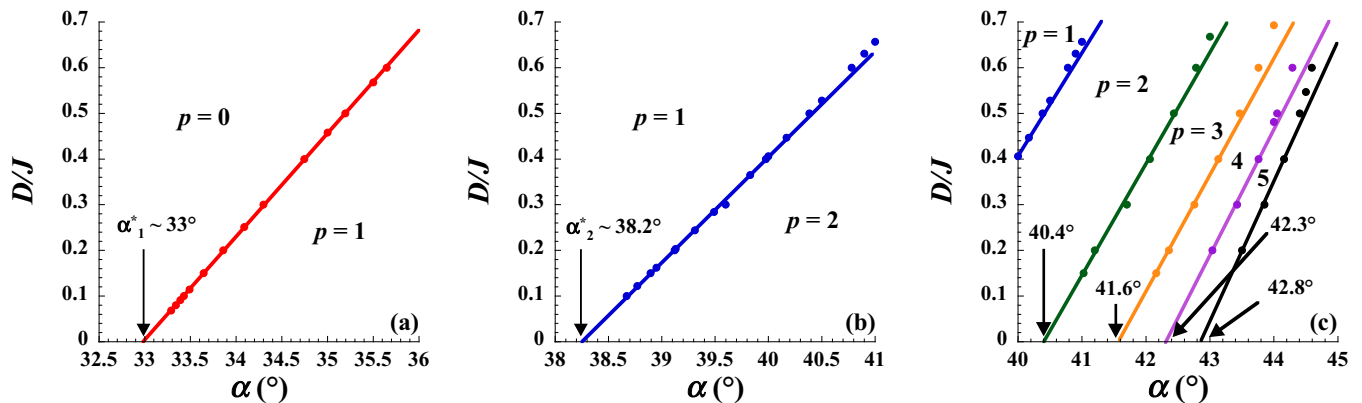


FIG. 19. Expanded view of the transition lines when D/J goes to zero. The extrapolation is consistent with the one obtained from the empirical expression [Eq. (E12)] of Appendix E. The different p values for the stable solution are also given.

V. CONCLUDING REMARKS

As emphasized in this work, the existence of DWs is the key ingredient to understanding the physics of anisotropic spin chains. In all cases, the D/J ratio is the relevant parameter to describe the different simple limits. On one hand, narrow DWs are found when the anisotropy is strong compare to the exchange energy ($D \gg J$). In particular, the existence of “strictly narrow” DWs, when $D/J > 4/3$, is a characteristic of the ferromagnetic chain but more complex DW profiles are always found for mixed or canted spin chains. On the other hand, broad DWs are found when the anisotropy is small ($D \ll J$) and a continuous approximation has been used to deduce an analytical expression of their profile. In this work, we went one step further by using a numerical method to obtain the characteristics (profile and energy) of the DWs in the general case.

A particularly rich discussion has emerged in the canted spin chain case, where a cascade of phase transitions has been described when the canting angle increases. Although confined to canting angles very close to 45° when the anisotropy is strong, the transition lines appear in a much broader window of canting angles for $D < J$. Subtle modifications of the profiles are found going through the observed transition lines. We have found, both numerically and analytically, that the energy difference between the different profiles is very small, typically of the order $2\pi^2 JS^2 \exp(-\pi^2/a)$ (see Appendix E). Even when D and J are comparable, this energy difference remains small, of the order of $JS^2/1000$, and is therefore smaller than $k_B T$ for experimentally relevant temperatures. This remark suggests that the thermodynamic properties of these canted chains may be affected. Quite generally, the equilibrium state of a spin chain consists of large domains of oriented spins separated by DWs. At low temperature, when $k_B T$ is much smaller than the energy of a DW, the correlation length is large and shows an activated behavior. In a simple description, valid in the Ising limit, the corresponding activation energy is simply the creation energy of the DW. However, it has been shown that this activation energy can be renormalized by the existence of spin waves, which add new fluctuations in the calculation of the free energy [42,43]. Although this argument should be still valid in the canted case, one may imagine

that fluctuations of the DW core may bring an additional contribution to the renormalization of the activation energy. Therefore, thermodynamic and dynamic properties of canted chains must eventually be revisited in the light of the present results.

Finally, our work suggests that further experimental and theoretical studies on more complex chains may be useful and lead to unique physical properties. For example, “mixed canted spin chains” (as defined in Secs. II and III) and their magnetic properties have been already reported in the literature [44–48]. These 1D systems could exhibit a combination of the results found for the mixed and canted spin chains and in particular a cascade of phase transitions might be experimentally observed. As illustrated by this work, these one-dimensional spin systems and their experimental realization thanks to advanced coordination chemistry offer to physicists a unique playground to discover interesting phenomena and exotic physics.

ACKNOWLEDGMENTS

This study has been carried out with financial support from the Centre National de la Recherche Scientifique (CNRS), the Université de Bordeaux, the region Nouvelle Aquitaine, the GdR MCM-2 (Magnétisme et Commutation Moléculaires) and the MOLSPIN COST action CA15128. We like to acknowledge fruitful discussions with A. Vindigni and the help of M. Rouzières in the design of the single-chain magnet 3D views.

APPENDIX A: DETAILS ON THE CRITICAL POINT AT $D/J = 4/3$

The starting expression of the energy, directly deduced from Eq. (3), is

$$\begin{aligned} \frac{\Delta E}{4JS^2} &= \frac{\cosh(\psi)}{2} + \frac{2 - \cosh(\psi)}{2} \cos(2\theta_0) \\ &+ \sum_{n=0}^{\infty} [1 - \cos(\theta_n - \theta_{n+1})] + [\cosh(\psi) - 1] \\ &\times \sum_{n=1}^{\infty} \sin^2(\theta_n). \end{aligned} \quad (\text{A1})$$

Equation (A1) can be developed up to fourth order:

$$\begin{aligned} \frac{\Delta E}{4JS^2} &= 1 + (\cosh(\psi) - 2)\theta_0^2 - \frac{\cosh(\psi) - 3}{3}\theta_0^4 \\ &+ \sum_{n=0}^{\infty} \left(\frac{(\theta_n - \theta_{n+1})^2}{2} - \frac{(\theta_n - \theta_{n+1})^4}{24} \right) \\ &+ [\cosh(\psi) - 1] \sum_{n=1}^{\infty} \left(\theta_n^2 - \frac{\theta_n^4}{3} \right). \end{aligned} \quad (\text{A2})$$

Introducing the exponential profile [Eq. (6)],

$$\begin{aligned} \frac{\overline{\Delta E}}{4JS^2} &= 1 + (e^\psi - 3)\frac{\theta_0^2}{2} \\ &+ \left(1 - \frac{(e^\psi - 1)^4 + 4e^{3\psi}(e^\psi - 1)^2}{8(e^{4\psi} - 1)} \right) \frac{\theta_0^4}{3}. \end{aligned} \quad (\text{A3})$$

This development describes a second-order phase transition located for $\exp(\psi) = 3$, or $D/J = 4/3$. Close to the critical point, the coefficient of the fourth order term can be taken at the critical value and the development approximated to:

$$\frac{\overline{\Delta E}}{4JS^2} \approx 1 + (e^\psi - 3)\frac{\theta_0^2}{2} + \frac{\theta_0^4}{10} \quad (\text{A4})$$

Consistent with the numerical result (if the angle is expressed in radians), this gives the equilibrium θ_0 value:

$$\bar{\theta}_0 = \sqrt{\frac{5}{2}(3 - e^\psi)}. \quad (\text{A5})$$

APPENDIX B: NUMERICAL METHOD

Our numerical approach consists of the resolution of a system of equations found at equilibrium thanks to an iterative Newton-Raphson method for a given D/J value. Taking the example of the regular ferromagnetic chain, this method refines a starting DW's profile of $(2N + 2)$ spins by increasing N until the result becomes independent of the chain size. The p -times-refined profile is contained in the vector x_p given in Eq. (B1):

$$x_p = \begin{pmatrix} \theta_{-N-1} \\ \vdots \\ \theta_N \end{pmatrix}. \quad (\text{B1})$$

To access to the x_p vector, each equation to solve is noted f_n as explicated in Eq. (B2):

$$f_n = \sin(\theta_n - \theta_{n+1}) + \sin(\theta_n - \theta_{n-1}) + \frac{D}{2J} \sin(2\theta_n). \quad (\text{B2})$$

These equations are gathered in the vector F_p [Eq. (B3)]:

$$F_p = \begin{pmatrix} f_{-N-1} \\ \vdots \\ f_N \end{pmatrix}. \quad (\text{B3})$$

The p th and $(p + 1)$ th steps are linked by Eq. (B4):

$$F_{p+1} = F_p + F'_p(x_{p+1} - x_p). \quad (\text{B4})$$

The refinement process consists of computing the vector $X_p = x_{p+1} - x_p$ for which the condition $F_{p+1} = 0$ is satisfied

[Eq. (B5)], with F'_p being the Jacobian matrix defined as $F'_p(i, j) = \partial F_p(i) / \partial x_p(j)$,

$$X_p = -(F'_p)^{-1} F_p. \quad (\text{B5})$$

The matrix inversion is generally an expensive calculation in term of computational time. Therefore, alternatively, the linear system given in Eq. (B6) has been solved to obtain the X_p vector,

$$F'_p X_p = -F_p. \quad (\text{B6})$$

Following these steps, the DW profile was refined until each $|f_n|$ values becomes smaller than the convergence criterion $\varepsilon_F = 1 \times 10^{-4}$. Then ΔE_N , the energy of the DW composed of $(2N + 2)$ spins, was calculated by substituting the refined profile in the Eq. (3). In order to avoid any finite-size effect in the determination for the DW's profile and energy, the procedure was repeated for larger N values. We considered that the finite number of spins involved in the calculation does not affect the DW properties as soon as the convergence criterion $\varepsilon_{\Delta E} = |\Delta E_N - \Delta E_{N-1}| / \Delta E_N$ is less than 1×10^{-3} . To ensure a quick convergence of the numerical method, each calculation starts from a D/J value where the DW's profile is analytically known. Then small variations of D/J were applied and we used the previous solution profile as the starting one for these new conditions. In this way, we took benefit of the continuous evolution of the DW's profile with the D/J ratio to perform calculations between the two limits.

APPENDIX C: MIXED CHAIN WITH QUANTUM SPINS

Considering the isotropic spins as quantum and interspin antiferromagnetic interactions, the Hamiltonian of the mixed chain is given by Eq. (C1), where \vec{e}_n is the unitary vector parallel to $(\vec{S}_n + \vec{S}_{n+1})$, which represents the quantification direction to diagonalize the independent Hamiltonians H_n ,

$$H = \sum_{-\infty}^{+\infty} H_n = 2|J| \sum_{-\infty}^{+\infty} |\vec{S}_n + \vec{S}_{n+1}| \vec{e}_n \cdot \vec{s}_n - DS^2 \sum_{-\infty}^{+\infty} \sin^2(\theta_n). \quad (\text{C1})$$

Moreover, as discussed by Seiden [49],

$$|\vec{S}_n + \vec{S}_{n+1}| = 2S \cos\left(\frac{\theta_n - \theta_{n+1}}{2}\right). \quad (\text{C2})$$

Then, the corresponding lowest eigenenergy for H_n is

$$\varepsilon_n = -4|J|Ss \cos\left(\frac{\theta_n - \theta_{n+1}}{2}\right) + DS^2 \sin^2(\theta_n) \quad (\text{C3})$$

Therefore, the chain energy expressed as a function of θ_n is the same [Eqs. (16) and (C3)] when considering classical or quantum s_i spins.

APPENDIX D: SMALL D/J LIMIT FOR THE CANTED CHAIN, THE CONTINUOUS APPROXIMATION

The starting point for this discussion is Eq. (31), in which variables ω_n and γ_n [Eq. (D1)] can be introduced in order to

obtain Eq. (D2) considering Eqs. (30) and (35),

$$\omega_n = \frac{\phi_n + \theta_n}{2} = \frac{\delta\phi_n + \delta\theta_n}{2}, \quad \gamma_n = \frac{\delta\phi_n - \delta\theta_n}{2}, \quad (\text{D1})$$

$$\begin{aligned} \frac{\Delta E}{4JS^2 \cos(2\theta_e)} = & \sum_{n=-\infty}^{+\infty} \left(1 - \frac{\cos(2\gamma_n) + \cos(\omega_{n+1} - \omega_n + \gamma_{n+1} + \gamma_n)}{2} + 2\sinh^2\left(\frac{\psi'}{4}\right) [\sin^2(\omega_n) + \sin^2(\gamma_n) \cos(2\omega_n)] \right. \\ & \left. - \frac{\tan(2\theta_e)}{2} [\sin(2\gamma_n) + \sin(\omega_{n+1} - \omega_n + \gamma_{n+1} + \gamma_n) - 2\cos(2\omega_n) \sin(2\gamma_n)] \right). \end{aligned} \quad (\text{D2})$$

This expression [Eq. (D2)] can be simplified, introducing $a = 4 \sinh(\psi'/4)$ and $\tan(2\theta_e) = ka/4$. Selecting the terms up to the second order in a gives Eq. (D3), in which a and k are independent parameters (close to $\alpha = 45^\circ$, k is much larger than a),

$$\frac{\Delta E}{4JS^2 \cos(2\theta_e)} = \sum_{n=-\infty}^{+\infty} \left[\bar{\gamma}_n^2 + \left(\frac{1}{2} \frac{d\omega_n}{dn} + \bar{\gamma}_n \right)^2 + \frac{a^2}{8} \sin^2(\omega_n) - \frac{ka}{4} \left(4\bar{\gamma}_n \sin^2(\omega_n) + \frac{1}{2} \frac{d\omega_n}{dn} \right) \right]. \quad (\text{D3})$$

For small values of D/J , the profile becomes very broad and the discrete sum of Eq. (D3) can be approximated by a sum of integrals to give Eq. (D4) (where ω and γ are the variables corresponding to ω_n and γ_n in the continuous limit):

$$\frac{\Delta E}{4JS^2 \cos(2\theta_e)} = \int \left\{ \gamma^2 + \left(\frac{1}{2} \frac{d\omega}{dn} + \gamma \right)^2 \right\} dn + \frac{a^2}{8} \int \{\sin^2 \omega\} dn - \frac{ka}{4} \int \left\{ 4\gamma \sin^2 \omega + \frac{1}{2} \frac{d\omega}{dn} \right\} dn. \quad (\text{D4})$$

At this approximation, an exact determination of the DW profile and its associated energy can be obtained. Minimization of Eq. (D4) with respect to γ gives Eq. (D5):

$$\bar{\gamma} = -\frac{1}{4} \frac{d\omega}{du} + \frac{ka}{4} \sin^2(\omega). \quad (\text{D5})$$

Thus $\bar{\gamma}$ can be introduced in Eq. (D4) to obtain an effective energy, Eq. (D6), depending only on ω :

$$\frac{\Delta \tilde{E}}{4JS^2 \cos(2\theta_e)} = \int \left(\frac{1}{8} \left(\frac{d\omega}{dn} \right)^2 + \frac{a^2}{8} \sin^2(\omega) [1 - k^2 \sin^2(\omega)] - \frac{ka}{4} \left(\frac{1}{2} - \sin^2(\omega) \right) \frac{d\omega}{dn} \right) dn. \quad (\text{D6})$$

The two a and k parameters allow a simplification of the calculations, as they are independent and directly related to D/J and α . For example, for small D/J and α values close to 45° , a and k can be approximated to Eqs. (D7) and (D8):

$$a \approx 2\sqrt{\frac{D}{J} \left(\frac{D}{4J} + \cos(2\alpha) \right)}, \quad (\text{D7})$$

$$k \approx \sqrt{\frac{\frac{D}{4J}}{\frac{D}{4J} + \cos(2\alpha)}}. \quad (\text{D8})$$

These results show the existence of a crossover due to the competition between two small parameters: D/J and $(45 - \alpha)$. When $D/J \gg \cos(2\alpha)$, k remains close to 1 and therefore much larger than a for small values of D/J . Equation (D6) can be even more simplified noting that the integral of the last term (proportional to ka) cancels due to the boundary conditions. Minimization of the remaining terms with respect to ω is straightforward and leads to Eq. (D9):

$$\frac{d^2 \bar{\omega}}{dn^2} = \frac{a^2}{2} \sin(2\bar{\omega}) [1 - 2k^2 \sin^2(\bar{\omega})]. \quad (\text{D9})$$

An exact double integration of Eq. (D9) is possible and, using Eq. (D5), gives:

$$\begin{aligned} \tan(\bar{\omega}) &= \frac{1}{\sqrt{1-k^2}} \frac{1}{\sinh(an)} \\ \bar{\gamma} &= \frac{\sqrt{1-k^2} \cosh(an) + k}{4[1 + (1-k^2)\sinh^2(an)]} a. \end{aligned} \quad (\text{D10})$$

APPENDIX E: SMALL D/J LIMIT FOR THE CANTED CHAIN CONSIDERING THE TWO KINDS OF DW PROFILES

As seen from numerical results, two kinds of equilibrium profiles are obtained. In the first case, later called ‘‘odd solution’’ (already discussed in Appendix D), the first spin after the center of the DW is a θ one. In the second one, later called ‘‘even solution,’’ this spin is a ϕ one. In other words, going from odd to even solutions is realized changing θ_e into $-\theta_e$ or k into $-k$. Then, a general description of the DWs energy, after minimization with respect to γ , is given by Eq. (44), with $\varepsilon = 1$ or -1 for odd or even solutions respectively. Returning to the initial expression of the energy in terms of a discrete sum, the energy difference between the $\varepsilon = 1$ and -1 profiles is given by Eq. (E1):

$$\frac{\Delta E_{1/-1}}{4JS^2 \cos(2\theta_e)} = -\frac{ka}{2} \sum_{n=-\infty}^{+\infty} \left(\frac{1}{2} - \sin^2(\omega_n) \right) \frac{d\omega_n}{dn}. \quad (\text{E1})$$

As the function to be summed is slowly varying with n , a standard approximation consists in considering n as a continuous function in order to replace the discrete sum by an integral. However, the corresponding integral is null and this approximation fails to describe the existence of a cascade of phase transitions with an alternation of odd and even profiles as shown by numerical results.

To go beyond the continuous approximation, a mathematical identity called Poisson summation can be used [50]. For an

real function $f(n)$, the Poisson identity is given by Eq. (E2):

$$\sum_{n=-\infty}^{+\infty} f(n) = \int_{-\infty}^{+\infty} f(u) du + 2 \sum_{s=1}^{+\infty} \int_{-\infty}^{+\infty} f(u) \cos(2\pi s u) du. \quad (\text{E2})$$

When $f(n)$ is varying slowly with n , the Fourier transform of f , which appears in the right part of Eq. (E2), varies quickly with s and the sum on s quickly converges. Thus the expression can be simplified, keeping only the $s = 0$ and $s = 1$ terms. The $s = 0$ term, which is the integral of the standard approximation [first term in the right part of Eq. (E2)], gives in our case no contribution. Then, simple expressions [Eqs. (E3) or E4] are obtained for the energy difference between $\varepsilon = +1$ and -1 :

$$\frac{\Delta \bar{E}_{1/-1}}{4JS^2 \cos(2\theta_e)} = -ka \int_{-\infty}^{+\infty} \left(\frac{1}{2} - \sin^2(\omega) \right) \times \frac{d\omega}{du} \cos(2\pi u) du, \quad (\text{E3})$$

$$\frac{\Delta \bar{E}_{1/-1}}{4JS^2 \cos(2\theta_e)} = -\frac{ka}{2} \int_{-\infty}^{+\infty} \cos(2\omega) \frac{d\omega}{du} \cos(2\pi u) du. \quad (\text{E4})$$

To estimate the above integral, the analytical profile, given by Eq. (39a), is introduced in order to express $\sin(2\omega)$ [Eq. (E5)] and thus $-\cos(2\omega)d\omega/du$ [Eq. (E6)] with $C = k^2/(1 - k^2)$:

$$\begin{aligned} \sin(2\omega) &= \frac{2\sqrt{1-k^2} \sinh(au)}{\cosh^2(au) - k^2 \sinh^2(au)} \\ &= \frac{2 \sinh(au)}{\sqrt{1-k^2} [\cosh^2(au) + C]}, \end{aligned} \quad (\text{E5})$$

$$\begin{aligned} -\cos(2\omega) \frac{d\omega}{du} &= \frac{a \cosh(au)}{\sqrt{1-k^2} [\cosh^2(au) + C]} \\ &\times \left(1 - \frac{2(1+C)}{[\cosh^2(au) + C]} \right). \end{aligned} \quad (\text{E6})$$

The energy difference is thus given by Eq. (E7):

$$\begin{aligned} \frac{\Delta \bar{E}_{1/-1}}{4JS^2 \cos(2\theta_e)} &= \frac{ka^2}{2\sqrt{1-k^2}} \int_{-\infty}^{+\infty} \frac{\cosh(au) \cos(2\pi u)}{\cosh^2(au) + C} \\ &\times \left(1 - \frac{2(1+C)}{[\cosh^2(au) + C]} \right) du. \end{aligned} \quad (\text{E7})$$

The obtained integrals are readily calculated [Eqs. (E8) and (E9)] from tabulated integrals [51] for $a \ll \pi^2$ and with $C = \sinh^2(\lambda/2)$. Thus, Eq. (E7) can be simplified to Eq. (E10):

$$\begin{aligned} I &= \int_{-\infty}^{+\infty} \frac{\cosh(au) \cos(2\pi u)}{\cosh^2(au) + C} du \\ &\approx \frac{2\pi}{a \cosh(\lambda/2)} \cos\left(\frac{\pi\lambda}{a}\right) e^{-\pi^2/a}, \end{aligned} \quad (\text{E8})$$

$$\begin{aligned} -\frac{dI}{dC} &= \int_{-\infty}^{+\infty} \frac{\cosh(au) \cos(2\pi u)}{[\cosh^2(au) + C]^2} du \\ &= -\frac{2}{\sinh(\lambda)} \frac{dI}{d\lambda} \\ &\approx \frac{4\pi e^{-\frac{\pi^2}{a}}}{a \cosh(\lambda/2) \sinh(\lambda)} \left(\frac{\pi}{a} \sin\left(\frac{\pi\lambda}{a}\right) \right. \\ &\quad \left. + \frac{1}{2} \tanh(\lambda/2) \cos\left(\frac{\pi\lambda}{a}\right) \right), \end{aligned} \quad (\text{E9})$$

$$\frac{\Delta \bar{E}_{1/-1}}{4JS^2 \cos(2\theta_e)} \approx -2\pi^2 e^{-\pi^2/a} \sin\left(\frac{\pi\lambda}{a}\right). \quad (\text{E10})$$

It should be noted that k and λ are related by $k = \tanh(\lambda/2)$ or $\lambda = \ln[(1+k)/(1-k)]$. For small values of D/J , θ_e remains small and an equivalent expression of Eq. (E10) is given in Eq. (E11):

$$\frac{\Delta \bar{E}_{1/-1}}{4JS^2} \approx -2\pi^2 e^{-\pi^2/a} \sin\left(\frac{\pi\lambda}{a}\right). \quad (\text{E11})$$

This result suggests to plot numerical results in a reduced form, to probe the existence of a master curve, namely to plot $y = (\Delta \bar{E}_{1/-1}/4JS^2)e^{\pi^2/a}$ as a function of $x = \pi\lambda/a$. The result is given in the main text. A master curve, shown in Fig. 17, is in fact obtained for D/J values up to 0.6. Remarkably, the above simple result $y \approx -2\pi^2 \sin(x)$ is even able to quantitatively reproduce the numerical data for large values of x , when $k \gg a$. An empirical function [Eq. (E12)] has been used to simulate the numerical data for any values of x :

$$y = -2\pi^2 \left(\sin(x) + 1.25 \frac{\sin(x) - x \cos(x)}{x^2} \right). \quad (\text{E12})$$

This expression is equivalent to the calculated simple result [Eq. (E11)] for large values of x . It should be noted that the analytical determination of the DW profile [Eqs. (39a) and (45)] is fully consistent when $k^2 a^2$ can be considered as a second-order term in a in Eq. (38), i.e., when $k \gg a$. This limit is effectively reached when k is close to 1, i.e., when x is large. Small departures in the profile expression may be present to explain that the above simple result may then be approximate when x is not large enough. Either with the simple limit or with the more general empirical expression, an oscillating function $y(x)$ is obtained. This describes a cascade of phase transitions, which takes place when $y = 0$. In the limit where D/J goes to zero, λ becomes close to $2k$ and x goes to $2\pi k/a$, which reduces to $\pi \tan(2\alpha)/2$. Introduced in the above expression of y [Eq. (E12)], the extrapolation of the canting angle values is possible at the transition lines, when D/J goes to zero. These extrapolations are also shown in Figs. 18 and 19. For example, for the $p = 0/p = 1$ phase transition, the canting angle extrapolates at about 33° .

More generally, the above analysis can be used to deduce the equation of the transition lines ($\alpha, D/J$). The existence of a $y(x)$ master curve implies that the transition lines correspond to $x = cst$, where the x values correspond to the zeros of the above empirical expression [Eq. (E12)]. This conclusion was checked to be consistent with the numerical results.

- [1] For recent reviews, see, for example, C. Coulon, H. Miyasaka, and R. Clérac, *Struct. Bonding (Berlin)* **122**, 163 (2006); C. Coulon, V. Pianet, M. Urdampilleta, and R. Clérac, *ibid.* **164**, 143 (2015).
- [2] A. Caneschi, D. Gatteschi, N. Lalioli, C. Sangregorio, R. Sessoli, G. Venturi, A. Vindigni, A. Rettori, M. G. Pini, and M. A. Novak, *Angew. Chem. Int. Ed.* **40**, 1760 (2001).
- [3] R. Clérac, H. Miyasaka, M. Yamashita, and C. Coulon, *J. Am. Chem. Soc.* **124**, 12837 (2002).
- [4] L. J. de Jongh, *J. Appl. Phys.* **53**, 8018 (1982).
- [5] H. J. M. de Groot and L. J. de Jongh, *Physica B* **141**, 1 (1986).
- [6] T. Sakai, M. Matsumoto, K. Asakura, and M. Sato, *Prog. Theor. Phys. Suppl.* **159**, 308 (2005).
- [7] M. Lakshmanan, B. Subash, and A. Saxena, *Phys. Lett. A* **378**, 1119 (2014).
- [8] K. Nakamura and T. Sasada, *Solid Stat. Commun.* **21**, 891 (1977).
- [9] J. F. Currie, J. A. Krumhansl, A. R. Bishop, and S. E. Trullinger, *Phys. Rev. B* **22**, 477 (1980).
- [10] T. Schneider, *Phys. Rev. B* **24**, 5327 (1981).
- [11] W.-M. Liu, X.-B. Wang, F.-C. Pu, and N.-N. Huang, *Phys. Rev. E* **55**, 1375 (1997).
- [12] S. Davis and G. Gutierrez, *Physica B* **355**, 1 (2005).
- [13] B. Barbara, *J. Phys.* **34**, 1039 (1973).
- [14] B. Barbara, *J. Magn. Magn. Mater.* **129**, 79 (1994).
- [15] H. Miyasaka, T. Madanbashi, K. Sugimoto, Y. Nakazawa, W. Wernsdorfer, K. Sugiura, M. Yamashita, C. Coulon, and R. Clérac, *Chem. Eur. J.* **12**, 7029 (2006).
- [16] N. Ishii, T. Ishida, and T. Nogami, *Inorg. Chem.* **45**, 3837 (2006).
- [17] M. Balanda, M. Rams, S. K. Nayak, Z. Tomkowicz, W. Haase, K. Tomala, and J. V. Yakhmi, *Phys. Rev. B* **74**, 224421 (2006).
- [18] Z. Tomkowicz, M. Rams, M. Balanda, S. Foro, H. Nojiri, Y. Krupskaya, V. Kataev, B. Büchner, S. K. Nayak, J. V. Yakhmi, and W. Haase, *Inorg. Chem.* **51**, 9983 (2012).
- [19] R. Ishikawa, K. Katoh, B. K. Breedlove, and M. Yamashita, *Inorg. Chem.* **51**, 9123 (2012).
- [20] J. H. Yoon, K. S. Lin, D. W. Ryu, W. R. Lee, S. W. Yoon, B. J. Suh, and C. S. Hong, *Inorg. Chem.* **53**, 10437 (2014).
- [21] M. Rams, E. V. Peresypkina, V. S. Mironov, W. Wernsdorfer, and K. E. Vostrikova, *Inorg. Chem.* **53**, 10291 (2014).
- [22] E. V. Peresypkina, A. M. Majcher, M. Rams, and K. E. Vostrikova, *Chem. Commun.* **50**, 7150 (2014).
- [23] M. G. F. Vaz, R. A. Allao, H. Akpinar, J. A. Schlueter, P. M. Lahti, and M. A. Novak, *Chem. Eur. J.* **20**, 5460 (2014).
- [24] R. A. Allao Cassaro, S. G. Reis, T. S. Araujo, P. Lahti, M. A. Novak, and M. G. F. Vaz, *Inorg. Chem.* **54**, 9381 (2015).
- [25] Z.-M. Sun, A. V. Prosvirin, H.-H. Zhao, J.-G. Mao, and K. R. Dunbar, *J. Appl. Phys.* **97**, 10B305 (2005).
- [26] A. V. Pali, O. S. Reu, S. M. Ostrovsky, S. I. Klokishner, B. S. Tsukerblat, Z.-M. Sun, J.-G. Mao, A. V. Prosvirin, H.-H. Zhao, and K. R. Dunbar, *J. Am. Chem. Soc.* **130**, 14729 (2008).
- [27] K. Bernot, J. Luzon, R. Sessoli, A. Vindigni, J. Thion, S. Richeter, D. Leclercq, J. Larionova, and A. Van Der Lee, *J. Am. Chem. Soc.* **130**, 1619 (2008).
- [28] C.-I. Yang, P.-H. Chuang, and K.-L. Lu, *Chem. Commun.* **47**, 4445 (2011).
- [29] I. Bhowmick, E. A. Hillard, P. Dechambenoit, C. Coulon, T. D. Harris, and R. Clérac, *Chem. Commun.* **48**, 9717 (2012).
- [30] M. Ding, B. Wang, Z. Wang, J. Zhang, O. Fuhr, D. Fenske, and S. Gao, *Chem. Eur. J.* **18**, 915 (2012).
- [31] J.-P. Zhao, Q. Yang, Z.-Y. Liu, R. Zhao, B.-W. Hu, M. Du, Z. Chang, and X.-H. Bu, *Chem. Commun.* **48**, 6568 (2012).
- [32] W.-X. Zhang, T. Shiga, H. Miyasaka, and M. Yamashita, *J. Am. Chem. Soc.* **134**, 6908 (2012).
- [33] S. Richeter, J. Larionova, J. Long, A. Van Der Lee, and D. Leclercq, *Eur. J. Inorg. Chem.* **2013**, 3206 (2013).
- [34] Q. Zhang, H. Zhang, S. Zeng, D. Sun, and C. Zhang, *Chem. Asian J.* **8**, 1985 (2013).
- [35] L.-H. Jia, Y.-J. Wang, C. Gao, M. Ding, J.-H. Jia, B.-W. Wang, and S. Gao, *Chem. Asian J.* **9**, 2463 (2014).
- [36] L. Su, W.-C. Song, J.-P. Zhao, and F.-C. Liu, *Chem. Commun.* **52**, 8722 (2016).
- [37] Z.-S. Cai, M. Ren, S.-S. Bao, N. Hoshino, and T. Akutagawa, *Inorg. Chem.* **53**, 12546 (2014).
- [38] V. Pianet, M. Urdampilleta, T. Colin, R. Clérac, and C. Coulon, *Phys. Rev. B* **94**, 054431 (2016).
- [39] See, for example, *The Landau Theory of Phase Transitions: Application to Structural, Incommensurate, Magnetic and Liquid Crystal Systems*, edited by J. Tolédano and P. Tolédano (World Scientific, Singapore, 1987).
- [40] V. Pianet, Ph.D. thesis, Université de Bordeaux, 2014.
- [41] Here, we describe the simple case of canted chains, already realized experimentally. More complex cases with a larger number of easy axis orientations will not be considered.
- [42] B. Sangiorgio, T. C. T. Michaels, D. Pescia, and A. Vindigni, *Phys. Rev. B* **89**, 014429 (2014).
- [43] M. Scarrozza, A. Vindigni, P. Barone, R. Sessoli, and S. Picozzi, *Phys. Rev. B* **91**, 144422 (2015).
- [44] T. Kajiwara, M. Nakano, Y. Kaneko, S. Takaishi, T. Ito, M. Yamashita, A. Igashira-Kamiyama, H. Nojiri, Y. Ono, and N. Kojima, *J. Am. Chem. Soc.* **127**, 10150 (2005).
- [45] K. Bernot, J. Luzon, A. Caneschi, D. Gatteschi, R. Sessoli, L. Bogani, A. Vindigni, A. Rettori, and M. G. Pini, *Phys. Rev. B* **79**, 134419 (2009).
- [46] T. S. Venkatakrishnan, S. Sahoo, N. Bréfuel, C. Duhayon, C. Paulsen, A. L. Barra, S. Ramasesha, and J. P. Sutter, *J. Am. Chem. Soc.* **132**, 6047 (2010).
- [47] S. Sahoo, J. P. Sutter, and S. Ramasesha, *J. Stat. Phys.* **147**, 181 (2012).
- [48] M. G. F. Vaz, R. A. Allao, H. Akpinar, J. A. Schlueter, S. Santos Jr, P. M. Lahti, and M. A. Novak, *Inorg. Chem.* **51**, 3138 (2012).
- [49] J. Seiden, *J. Phys. Lett.* **44**, L947 (1983).
- [50] See, *Principles of the Theory of Solids*, 2nd ed., edited by J. M. Ziman (Cambridge University Press, London, 1972), p. 319.
- [51] See, *Table of Integrals, Series and Products*, 6th ed., edited by I. S. Gradshteyn, I. M. Ryzhik, and A. Jeffrey (Academic Press, San Diego, 2000), p. 507.